An Artificial Intelligence-Aided Robotic Platform for Ultrasound-Guided Transcarotid Revascularization

Giovanni Faoro, *Student Member, IEEE*, Sabina Maglio, Stefano Pane, Veronica Iacovacci, *Member, IEEE*, and Arianna Menciassi, *Fellow, IEEE*

***Abstract*—Transcarotid Artery Revascularization (TCAR) is typically performed by manual catheter insertion and implies radiation exposure for both the patient and the surgeon. Taking advantage from robotics and artificial intelligence (AI), this letter presents a robotic ultrasound (RUS) platform for improving the procedure. To this purpose, ultrasound (US) imaging is considered both in the pre-operative stage for procedure planning and in the intra-operative stage to track a catheter. 3D vascular volumes can be precisely reconstructed from sequences of 2D images exploiting robotic probe manipulation and AI-based image analysis. The method proved a median reconstruction error lower than 1 mm. Pre-operative information are mapped to the intra-operative scenario thanks to a US-based registration routine. The automatic probe alignment on the target vessel demonstrated to be as precise as 0.84°. The reconstructed 3D model can be exploited to automatically generate a catheter trajectory based on user inputs. Such trajectory enabled automatic insertion of a magnetic catheter steered by an external permanent magnet actuated by the RUS platform. Our results demonstrate a catheter tip target reaching error of 3.3 mm. We believe that these results can open the way for the introduction of robotics and AI in TCAR procedures enabling precise and automatic small-scale intravascular devices control.**

***Index Terms*—Robotic ultrasound, deep learning, vascular reconstruction, ultrasound imaging, magnetic catheter.**

I. Introduction

CAROTID artery stenosis is an important cause of stroke. Stroke is a major atherosclerotic cardiovascular disease and a leading cause of premature death worldwide [1], [2]. Patients with internal carotid artery (ICA) stenosis higher than 60% are typically considered eligible for surgery, which consists of gold standard endarterectomy or minimally invasive stenting interventions [2]. Minimally invasive procedures account mainly for transfemoral or transradial catheter insertion with the need to manually manipulate guidewires through tortuous paths. These approaches are characterized by high technical complexity setting the need for trained expert operators or for complex robotic insertion systems [3], [4], [5]. Most of the image-guided robotic catheter systems proposed so far suffer from the use of ionizing radiations for imaging and from non-efficient actuation. Concentric tube [6], hydraulic [7] or magnetic control have been proposed for catheter actuation and control. Among these solutions, magnetic control has gained popularity thanks to tissue transparency to magnetic field, real-time operation, fine and contactless control and miniaturization possibilities for the controlled magnetic device [8], [9], [10]. On the imaging side, the commonly exploited CT-based guidance proves expensive for the healthcare system, exposes both the patient and the surgeons to harmful ionizing radiations and has a relatively low frame rate. For these reasons, special attention has been paid toward ultrasound (US) imaging which is a low cost non-ionizing imaging technique with real-time performances. Interpreting US images is however non-straightforward, due to the presence of artifacts and noise. Deep learning (DL) methods have demonstrated their ability in tackling the complexity of medical image analysis, even in the tricky case of US [11], [12]. Recent studies revealed that achieving good quality results with relatively small datasets is also possible even in the most complex clinical scenarios. For example, exploiting VGG-UNet and transfer learning [13], [14] successfully tackled tumor segmentation tasks in magnetic resonance and US images. Nevertheless, the performances of DL algorithms largely depend on image quality, so on the operator when using US. Researchers have thus worked to develop Robotic US (RUS) systems, granting the acquisition of good quality real-time US images, without the need of an expert operator [15]. Additionally, the knowledge of the US probe pose, provided by the robotic arm at each image acquisition step, enabled 3D volume reconstructions from 2D images [16]. Several platforms have been proposed for automatic vascular diagnosis [17], [18], [19], [20] performing 3D vessel shape reconstruction and the assessment of stenosis, which is fundamental for decision making in therapy selection [21], [22], [23]. Anyway, low resolution and contrast of US images typically limit small-scale catheters or instruments tracking, hampering the performance of surgical procedures exclusively under US guidance. An interesting case study in this sense is transcarotid artery revascularization (TCAR), a novel clinical procedure for carotid artery stenting. Within this context, this study proposes a new US-based robotic platform targeting TCAR. Even though the platform presented here can be considered as general

Manuscript received 31 October 2022; accepted 20 February 2023. Date of publication 2 March 2023; date of current version 13 March 2023. This letter was recommended for publication by Associate Editor T. Xu and Editor P. Valdastri upon evaluation of the reviewers' comments. This work was supported in part by the European Union's Horizon 2020 Research and Innovation Programme under Grant 101017140 and in part by the European Union's Horizon 2020 Research and Innovation Programme under Marie Sklodowska-Curie under Grant 894425. *(Corresponding author: Giovanni Faoro.)*

Giovanni Faoro, Sabina Maglio, Stefano Pane, and Arianna Menciassi are with the BioRobotics Institute, Scuola Superiore Sant'Anna, 56127 Pisa, Italy, and also with the Department of Excellence in Robotics and AI, Scuola Superiore Sant'Anna, 56127 Pisa, Italy (e-mail: giovanni.faoro@santannapisa.it; sabina.maglio@santannapisa.it; stefa.pane@gmail.com; arianna.menciassi@santannapisa.it).

Veronica Iacovacci is with BioRobotics Institute, Scuola Superiore Sant'Anna, 56127 Pisa, Italy, also with the Department of Excellence in Robotics and AI, Scuola Superiore Sant'Anna, 56127 Pisa, Italy, and also with the Department of Mechanical and Automation Engineering, Chinese University of Hong Kong, Hong Kong (e-mail: veronica.iacovacci@santannapisa.it).

This letter has supplementary downloadable material available at https://doi.org/10.1109/LRA.2023.3251844, provided by the authors.

Digital Object Identifier 10.1109/LRA.2023.3251844

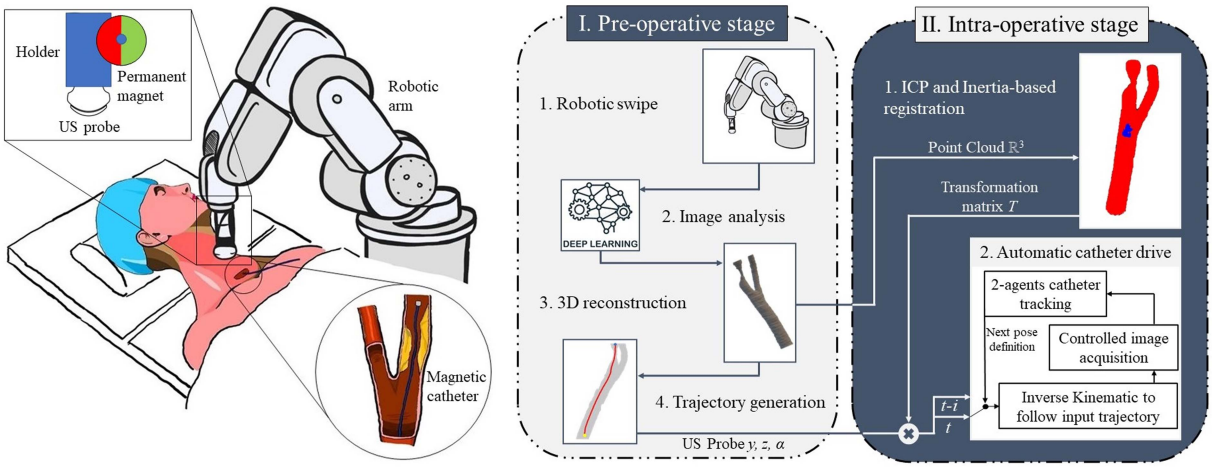

Fig. 1. Conceptual sketch of the RUS platform for TCAR procedure. The US probe and the permanent magnet, relatively fixed, are moved by a robotic arm to steer and track a magnetic catheter. On the right, a block diagram of the procedure. In the pre-operative phase, the robotic arm performs a predefined swipe acquiring a sequence of images of the scanned 3D workspace. A 3D vascular model is created exploiting AI and is then used to automatically generate a trajectory to bring the catheter tip from the insertion to the target point. During the intra-operative phase, a US-based registration routine is exploited to align the patient position with the pre-operative model and to refer it to the robot base frame. At this point, the robotic arm follows the predefined trajectory checking for catheter position at each trajectory point.

purpose for US-guided procedures, we decided to focus on TCAR since it is a catheterization procedure eligible to be carried out completely under US imaging in light of the superficial position of the involved vessel, namely the common carotid artery (CCA) in patient's neck. Although US imaging could be used for procedure planning and delivery, this is not currently done due to the limitations imposed by US in terms of its 2D nature, low contrast and resolution, difficult interpretability and the need for operator's hand-eye coordination to manipulate the catheter while optimally placing the US probe to image the target vessel. Thus, this procedure could benefit from robotics to overcome the 2D imaging limitation and for precise and automatic probe alignment and control. TCAR could also benefit from artificial intelligence (AI) to facilitate image analysis and interpretation, thus reducing surgeon burden and mental effort. To make robotics and AI beneficial for TCAR procedures, in this letter we propose a novel RUS platform including different technical blocks adopted in the pre- and intra-operative stages (Fig. 1). Robotic workspace scanning and DL image analysis enable precise 3D reconstruction of patient's CCA. A planning block is exploited to generate an optimal path to guide the catheter based on user-defined target point and this concludes the pre-operative stage. The intra-operative stage starts with a registration routine, allowing automatic probe alignment on the target vessel. Last, US images are used to track the magnetic catheter tip during automatic insertion guiding the catheter along the computed optimal trajectory.

The proposed RUS platform has some merits with respect to existing systems [8], [9], [24], [25] in light of the novelties introduced in the procedure and in the technical blocks associated to the platform. In particular:

- DL image analysis. The ability of VGG-UNet to tackle a different task from the ones explored in literature, as tumor segmentation [13], [14], is analyzed. Thanks to transfer learning, we faced vessel segmentation in both clinical and phantom images. Additionally, VGG-UNet first integration in a robotic platform is proposed.
- US-based registration. State-of-the-art US-based catheterization platforms do not address intra-operative automatic probe alignment on target vessel, which is a fundamental step for optimal imaging and planned trajectory following [8], [9], [24], [25]. Here, a custom image-based registration technique, exploiting AI-based reconstruction and inertia tensor formulation, has been developed to automatically align pre- and intra-operative scenarios.

Overall, the novelties and technical blocks introduced in this platform allowed us to simulate for the first time a TCAR procedure with a robotic approach.

The remainder of this letter is organized as follows. Section II presents an overview of the system, platform components are described in the first paragraph, followed by five paragraphs on the advanced US-based methods. Experimental results are reported in Section III, demonstrating platform performances in 3D vessel reconstruction, US-based registration and magnetic catheter guidance. Section IV concludes this letter.

II. Platform Overview and Advanced Methods for US-Based Catheter Guidance

This section provides details on the robotics and AI-enabled methods for US-based TCAR procedures. The implemented approach can be divided into pre- and intra-operative phases, as illustrated below and shown in Fig. 1.

The proposed robotic procedure is meant to start with an automatic US workspace scanning to precisely reconstruct patient 3D CCA model. This reconstruction can be used by the medical expert in the pre-operative phase to evaluate patient conditions and select the appropriate treatment. If the patient is considered eligible for TCAR, catheter insertion can be planned exploiting vascular reconstruction and vessel centerline. At the beginning of the procedure, the US-based registration routine allows to align the pre-operative model with current intra-operative patient position and to refer the model to the robot base frame. The robotic arm holds both the US probe and a permanent magnet

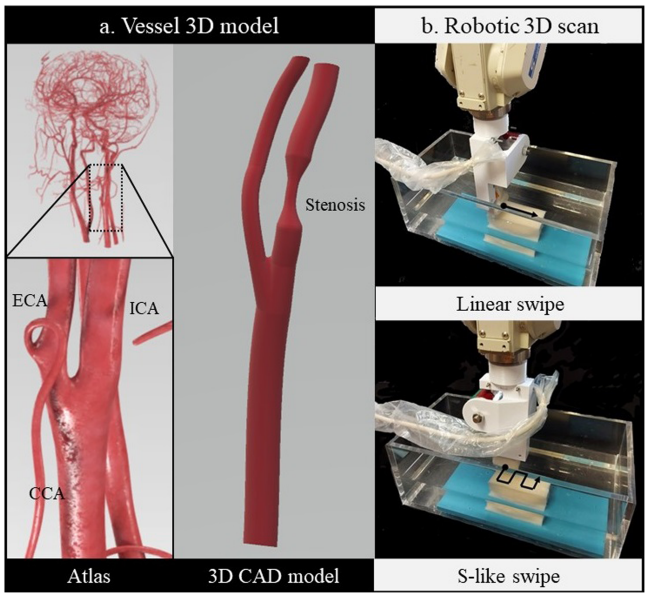

Fig. 2. Methods for 3D vascular reconstruction. In panel a) the surgical atlas, with focus on CCA, ECA and ICA, is shown, together with the designed CAD model with stenosis. In panel b) the robotic swipes used for 3D workspace scan are depicted.

rigidly connected to the arm end effector. The permanent magnet is used to remotely actuate a magnetic catheter intended to perform the procedure. As a consequence, the planned trajectory, defined as a sequence of robotic arm end effector poses, can be covered by the robotic system, automatically guiding a magnetic catheter toward the target location. US images enable catheter tip tracking at each trajectory point, to provide feedback information to the robotic arm about catheter motion.

A. Robotic Platform Hardware Components

The RUS platform consists of a six Degrees of Freedom (DoF) robotic arm (Melfa RV-3SB, Mitsubishi, Japan), a linear US probe (L15-7H40, Telemed, Lithuania) and a cylindrical permanent magnet (60 mm in diameter, 70 mm in height, NdFeB, diametral magnetization and grade N35). A custom holder was designed to allow simultaneous tracking and magnetic control of the catheter. The holder was designed (Fusion 360 software, Autodesk, USA MK3S) and prototyped through a 3D printer (Prusa Research, Czech Republic) to allow mounting both the US probe and the permanent magnet onto the robotic arm end effector.

The catheter consists of a biocompatible silicone rubber (PR 410/60) hollow tube with outer diameter of 2 mm. On its tip, 8 small cylindrical permanent magnets (2 mm in diameter, 1 mm in height, grade N48, axial magnetization) were attached to provide the catheter with magnetic properties.

A tissue mimicking phantom was used to simulate catheter insertion into the CCA. The phantom was realized as a bulk volume with a hollow vessel-shaped volume. The 3D model of regular CCA, external carotid artery (ECA) and ICA presenting a 60% stenosis was designed using Fusion 360 software and following as reference an online available surgical atlas [26] (Fig. 2(a)). Branches lengths and radii were set based on literature [27]. The model was provided with an interlock in the ECA branch to simplify vessel mold removal from the final phantom. The artery model has been 3D printed in UV-curable resin with PoliJet printing technique (3DSystems, USA). The vessel mold was then placed inside a rectangular mold in the desired position. To obtain the bulk volume, Agarose and Ployvinyl alcohol (PVA) powders (Sigma-Aldrich) were dissolved in a deionized and degassed water (dd-H2O)-soy milk (5% v/v) solution. The Agarose and PVA concentration was set to 2% v/v and 4% v/v, respectively, to replicate acoustic properties of human tissues, and to provide both elastic properties and structural integrity to the final phantom [28], [29]. The solution was then poured into the rectangular mold and physically crosslinked through freeze-thawing cycles (3 cycles, 16 hours per cycle). The vessel mold was then removed from the bulk volume producing the desired vessel-like cavity.

B. Deep Learning Based Vessel Detection

Several approaches have been proposed in literature for automatic vessel segmentation of US images. Methods range from phase symmetry [30], watershed transform [31], affinity propagation [32] and DL [33], [34]. DL methods are nowadays preferred over the others because of their higher generalization abilities and image analysis performances. One of the most common DL architectures for medical image segmentation is the U-Net, which is characterized by a contracting (encoder) and an expansion (decoder) path [35]. Here we considered one of its variations, VGG-UNet, which adopts VGG-16 architecture as contracting path. This is done to exploit VGG-16 weights pre-trained on the ImageNet dataset and then perform transfer learning to adapt the network to vessel segmentation, despite the use of a relatively small dataset. Such approach has been already adopted for medical image analysis, as in the case of MRI-based brain tumor or US-based breast cancer segmentation [13], [14]. On the other hand, its application to US-based carotid segmentation and integration into a RUS platform is still unexplored. The VGG-UNet convolutional neural network (CNN) is fed with 256 $\times$ 256 pixels images providing as output a 256 $\times$ 256 probability map, which represents segmentation output. The architecture is trained considering the Dice Loss, defined as 1-Dice Similarity Coefficient (DSC), which is computed as two times the cardinality of output and ground truth intersection over the sum of cardinalities.

Two small datasets, to be used for transfer learning, were collected: a phantom dataset and a clinical one. A US compatible phantom with a desired hollow tubular section was fabricated. The phantom had the same material composition as the CCA one used for testing but with a single 3 mm in diameter tubular cavity to mimic a vessel. This was done to avoid unwanted correlations between CNN dataset images and 3D reconstruction test ones, so to ensure unbiased 3D reconstruction results. A manual swipe was performed enabling the acquisition of 400 images both in the longitudinal and transversal vessel views, to allow the network to be robust with respect to different probe-vessel orientations. A clinical dataset of 240 CCA US images in the longitudinal and transversal views was collected from online repositories [36] to check for network usability in real-life scenarios. The images from the datasets had different sizes and were resized to 256 $\times$ 256 pixels. In both cases, gold-standard (GS) annotation was obtained semi-automatically by using GIMP environment (GNU Image Manipulation Program 2.10.28).

The CNN was implemented with TensorFlow and Keras libraries and ran on NVIDIA Tesla K80 GPU provided by

Google Collaboratory. The architecture was trained with Adam optimizer with a learning rate of 0.03, adapted during learning with an InverseTimeDecay routine. Batch size was set to 20 and the maximum number of epochs to 200, but EarlyStopping with a patience of 20 was used to avoid overfitting. A 5-fold cross-validation was used for robust testing. Training images were furtherly split upon shuffling, into training set (80%) and validation set (20%) and online data augmentation techniques, such as random rotation, zoom, shift and horizontal flip, were applied during training.

C. Robotic-aided 3D Vessel Reconstruction

The 2D nature of US imaging limits its direct use in applications in which 3D information is mandatory, as in the case of TCAR where the intravascular device has to be guided through a bifurcated vessel. To overcome these limitations, robotics for automatic scanning of 3D workspaces with position–controlled image acquisition can be exploited [16], [17], [18], [19], [20], [21], [22]. The robotic arm is controlled thanks to a custom Matlab Simulink Real-Time (version R2020a, The Mathworks Inc., Natick, MA) routine and follows a user-defined trajectory, either linear or s-like swipes (Fig. 2(b)), specified as a sequence of pose increments $\boldsymbol{\Delta}_i$. The robotic arm is guided, thanks to joystick commands, to a desired initial pose $\mathbf{p}_0 = [\mathrm{x}_0, \mathrm{y}_0, \mathrm{z}_0, \alpha_0, \beta_0, \gamma_0]$ and the sequence of increments is used to compute the new desired pose $\mathbf{p}_\mathrm{i}$ at each time step t_i following (1).

$$\boldsymbol{p_i} = \boldsymbol{p}_0 + \sum_i \boldsymbol{\Delta_i} t_i \tag{1}$$

Once a new trajectory point is reached, the robot controller sends an acquisition command via user datagram protocol (UDP) to the US probe C++ app (Visual Studio 2019) commanding for a new image acquisition. In this way, each stored image is associated to a precise spatial pose $\mathbf{p}_\mathrm{i}$. The US images are then fed to the CNN and the output segmentation maps are scaled with a pixel_to_mm coefficient given by probe features. The pose information associated to each image, and in particular the relative translation and rotation increments $\boldsymbol{\Delta}_i$, are then used to compute the relative transformation matrices $\mathbf{T}_\mathrm{i}$. Thanks to these $\mathbf{T}_\mathrm{i}$, the 2D images are mapped into the local US reference frame at time t_0 and stacked to reconstruct the 3D vasculature. Finally, as last reconstruction step, 3D vessel surface is smoothened by applying a 3D Gaussian filter.

D. Automatic Trajectory Generation

A precise patient-specific 3D vascular model can be exploited for image-guided intravascular device insertion, by allowing to estimate optimal trajectories for the catheter tip to reach a target location. In order to avoid vessel wall damages and to ensure optimal tool visualization, catheter trajectory should coincide with vessel centerline.

Here we took advantage of a state-of-the-art approach to estimate point clouds skeletons via Laplacian-based contraction [37]. This method provides an estimation of the vessel centerline from a reconstructed 3D volume, automatically managing vessel tortuousness and bifurcations. Once vascular centerline has been estimated, the user is required to select an insertion and target point on the 3D model via a graphical user interface (GUI), together with the desired advancement step *l*. The centerline is then split into different branches based on end and bifurcation points. The reference branch is selected as the one containing both the insertion and the target point and its projection on the *yz* plane is considered. This is done to focus on three US probe Degrees of Freedom (DoFs): out-of-plane translation, in-plane horizontal translation and out-of-plane rotation, i.e., rotation around probe longitudinal axis. These selected DoFs are the main ones contributing to the optimal US imaging of the vessel. A sketch on these controlled DoFs is shown in Fig. 3(a). The trajectory generation algorithm provides as output position increments for the robot encoder in the *yz* plane and roll angle α orientation increments, as explained in Algorithm 1.

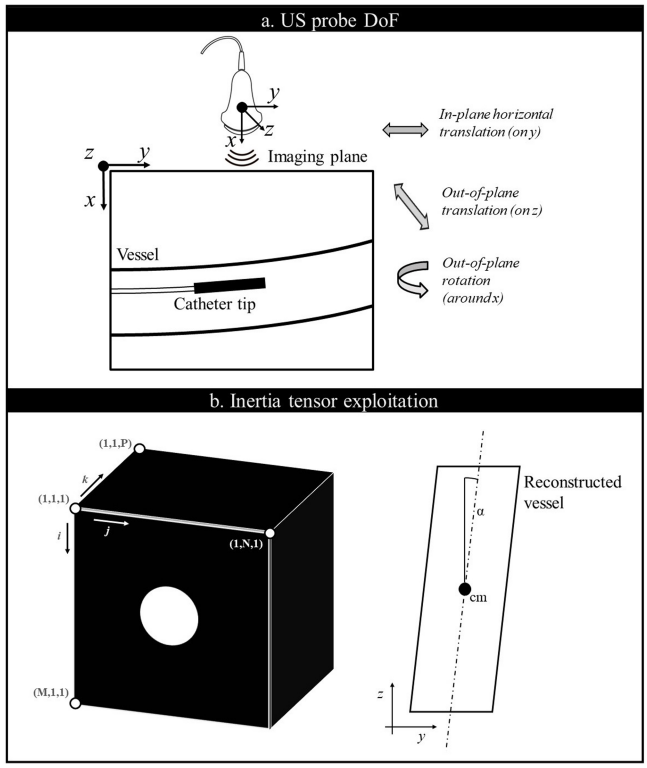

Fig. 3. In panel a) US probe controlled DoFs are depicted. Out-of-plane translation refers to translation on z, while in-plane translation refers to the one on y. In panel b), left side, a sketch representing the MxNxP reconstructed volume is depicted. On the right side, the projection of reconstructed vessel in *yz* plane is represented, showing the 2D position of volume center of mass (cm) and the out-of-plane angle α to be used to align the probe with the vessel longitudinal axis.

E. US-based Registration Routine

To link pre-operative model reconstruction with the intra-operative scene, in which vessel pose might have changed due to a different patient, bed or robot position, a registration step has to be performed. Here we developed a completely US-based registration routine to align the patient model with the robot base frame. A space sub-scan is performed to reconstruct a small vessel portion in the operative scenario. Iterative Point-Cloud (ICP) registration is firstly performed to align the reconstructed sub-volume with the complete pre-operative model. This allows the understanding of the current US probe position with respect to the pre-operative 3D model. Secondly, the relative position and orientation of the sub-volume with respect to the initial probe pose are computed, enabling automatic alignment of the

Algorithm 1: Path Planning for Catheter Tip.

Inputs:
$\mathbf{C} \in \mathbb{R}^{mx3}$: [*x*,*y*,*z*] vessel centerline points
$\mathbf{p_i} \in \mathbb{R}^3$: starting 3D insertion point selected by user
$\mathbf{p_t} \in \mathbb{R}^3$: final 3D target point selected by user
$\boldsymbol{l} \in \mathbb{R}$: point-to-point step
Output:
$\mathbf{p} \in \mathbb{R}^{nx3}$: [*y*,*z*,α] robotic end effector sequence of increments
Code:
Detect branches end-points and bifurcation
compute point-to-point distances d for each point
if(d $<\varepsilon$*) is true one time* $\rightarrow$ *end point*
two times $\rightarrow$ *central point*
three times $\rightarrow$ *bifurcation*
Create graph for each branch
for n times, where n = #end-points -1
  define end-point i as node
  search for closest point and create connection
  go on until another end-point is reached
Select optimal branch
compute distances of p_i *and* p_t *(*d_i *and* d_t*) from branches*
select branch with min(d_i+d_t*)*
upsample branch points by linear fitting between nodes
· Compute vector of position and orientation increments
for i = 2:length(branch)
  pos_incr[i-1] = branch[i]-branch[i-1]
  α*_incr[i-1] = atan2(pos_incr[i-1,y],pos_incr[i-1,z])*
Compute sequence of increments **p** to reach target $\mathbf{p_t}$
$p = p_i$
while(true)
  if(norm(p_t - *p)* $< l$*)* (we are close to target, so we reduce the step)
    $l = norm(p_t - p)$
  search for the point p with incremental distance closer to l and add it to trajectory
  if(norm(p_t - *p)* $>$ *norm(*$p_t - p_{-1}$*)* $\|$ *norm(*p_t - *p)* $<\xi$*)*
    $p = p_{-1}$
    break (we are moving away from target or we are closer than ξ)

probe with patient vasculature. The reconstructed sub-volume V is represented by an MxNxP volume (where M and N refer to single image dimensions and P to number of images), where voxels with value 0 indicate empty space and voxels with value 1 indicate vessel presence, as illustrated in Fig. 3(b). The vessel center can be estimated by computing sub-volume center of mass *CoM*, whereas vessel orientation can be derived by calculating sub-volume inertia tensor **I**, which formulation is provided in (2)–(6).

$$mass = \sum_{i=1}^{M}\sum_{j=1}^{N}\sum_{k=1}^{P} V(i,j,k) \tag{2}$$

$$CoM_x = \left(\frac{1}{mass}\right) * \sum_i \sum_j \sum_k i * V(i,j,k) \tag{3}$$

$$CoM_y = \left(\frac{1}{mass}\right) * \sum_i \sum_j \sum_k j * V(i,j,k) \tag{4}$$

$$CoM_z = \left(\frac{1}{mass}\right) * \sum_i \sum_j \sum_k k * V(i,j,k) \tag{5}$$

$$\mathbf{I} = \sum_{i=1}^{M}\sum_{j=1}^{N}\sum_{k=1}^{P} V(i,j,k) * [\boldsymbol{c}_1 | \boldsymbol{c}_2 | \boldsymbol{c}_3] \tag{6}$$

where

$$\boldsymbol{c}_1 = \begin{bmatrix} (j-CoM_y)^2 + (k-CoM_z)^2 \\ -(j-CoM_y)(i-CoM_x) \\ -(i-CoM_x)(k-CoM_z) \end{bmatrix},$$

$$\boldsymbol{c}_2 = \begin{bmatrix} -(j-CoM_y)(i-CoM_x) \\ (i-CoM_x)^2 + (k-CoM_z)^2 \\ -(j-CoM_y)(k-CoM_z) \end{bmatrix},$$

$$\boldsymbol{c}_3 = \begin{bmatrix} -(i-CoM_x)(k-CoM_z) \\ -(j-CoM_y)(k-CoM_z) \\ (j-CoM_y)^2 + (i-CoM_x)^2 \end{bmatrix}$$

Eigendecomposition of the symmetric inertia tensor **I** can be performed to estimate vessel major axes orientations and radius. Among the eigenvalues (λ_1, λ_2, λ_3) two should be equal and associated to the two orthogonal transversal axes. The remaining one is associated to the longitudinal vessel axis, thus enabling automatic recognition of the associated eigenvector. By trigonometry it is then possible to estimate probe out-of-plane rotation for optimal alignment. Additionally, vessel radius *r* can be estimated considering (7). This can be helpful to evaluate possible variations in vessel lumen dimensions between pre- and intraoperative scenarios, e.g., due to new plaque formation.

$$r = \sqrt{\frac{2\lambda}{mass}} \tag{7}$$

F. Magnetic Catheter Automatic Insertion

The trajectory generated pre-operatively and later registered on the real patient can be used in the intra-operative stage to follow the vascular structure in 3D and to allow for automatic catheter insertion. Magnetic catheter actuation relies on the interaction between the magnetic dipole ($\mathbf{m} \in \mathbb{R}^3$) associated to the catheter tip and the field ($\mathbf{B}(p) \in \mathbb{R}^3$) generated on a point in space ($p \in \mathbb{R}^3$) by an external magnetic source. In this platform, the magnetic field **B** is generated by a cylindrical permanent magnet fixed rigidly nearby the US probe. In this way, moving the robotic end effector to let the probe optimally follow the 3D vascular structure also ensures optimal positioning of the magnetic field source for catheter steering and control. To model magnet-catheter interactions, the dipole-dipole approximation was adopted, in light of the considered magnet dimensions and distances (magnet radius of 30 mm and magnet-catheter distance around 140 mm). This allowed us to theoretically validate the magnetic actuation strategy.

The permanent magnet is used to generate a torque $\boldsymbol{\tau}$ and a force **F** on the magnetic catheter tip to align it with the vessel centerline and drag it toward the target point, respectively. Their

formulation is reported in (8).

$$\begin{cases} \boldsymbol{\tau} = \boldsymbol{m} \times \boldsymbol{B} \\ \boldsymbol{F} = \boldsymbol{\nabla} (\boldsymbol{m} \cdot \boldsymbol{B}) \end{cases} \tag{8}$$

where $\times$ and $\cdot$ represent cross and dot product respectively and ∇ indicate field gradient.

In addition, to monitor the automatic catheter insertion, a 2-players tracking routine is implemented to detect catheter tip presence inside the US frame. First, a Region Of Interest (ROI) for catheter tip detection is generated by the first player by exploiting a correlation coefficient template matching method, similarly to what has been done in previous works [8], [9], [25]. However, template matching methods always output a ROI for the given image even though the object of interest might not be present. To be robust with respect to these errors, the ROI is then classified by the second player as containing or not the catheter, by exploiting image statistics. ROI mean, median, standard deviation and similarity with the template (computed as the sum of ROI-template pixel-to-pixel product) were visually inspected. Standard deviation and similarity metrics were selected as ROI features to develop a logistic regressor binary classifier. To train such classifier, two datasets, each composed by 250 images, were acquired by letting the system follow the automatic vessel centered trajectory in open-loop with and without the catheter. The classifier was then trained on 80% of the dataset considering gradient descent with a learning rate equal to 0.001 and 100000 iterations and then tested on the remaining 20%. During automatic catheter insertion, if the catheter tip is found, then the position is declared as safe (in the sense that the catheter is correctly following the planned trajectory) and the robotic arm moves to the next pose. If the catheter is not found for more than n consequent frames (where n is a safety margin to be set), then the robotic arm stops moving on and goes back to the most recent safe position. This control method represents a Variable Structure Binary Feedback control, in which the shift from one control law to the other (move on or go back) is determined by the binary feedback variable retrieved from catheter tracker.

III. Experimental Validation & Results

This section illustrates the evaluation of platform performance in terms of 3D vessel anatomy reconstruction fidelity, US-based registration efficiency, 2-players tracking routine performance and magnetic catheter closed-loop control errors. Experimental results are also shown in the ***Supporting Video***.

A. 3D Vascular Reconstruction

Reconstruction fidelity is fundamental to guarantee proper intra-operative catheter insertion, since automatic device control relies on the reconstructed model.

To objectively evaluate US-based reconstruction performances, the vessel CAD model is used as ground-truth. The AI-based reconstructed volume is aligned with the reference one through ICP registration. A distance map is computed considering Euclidean distance between corresponding points of the two point clouds. Correspondence between model points is assessed evaluating surface normal versors, so to penalize network faults in vessel boundaries detection. The CNN architecture reached an average DSC higher than 90% on both datasets, namely 92.96% on the clinical dataset and 95.05% on the phantom one and representative examples are shown in Fig. 4(a). In Fig. 4(b) the distance color map representing reconstruction performances on the CCA phantom is reported. The median reconstruction error is 0.95 mm with an interquartile range of 1.04 mm.

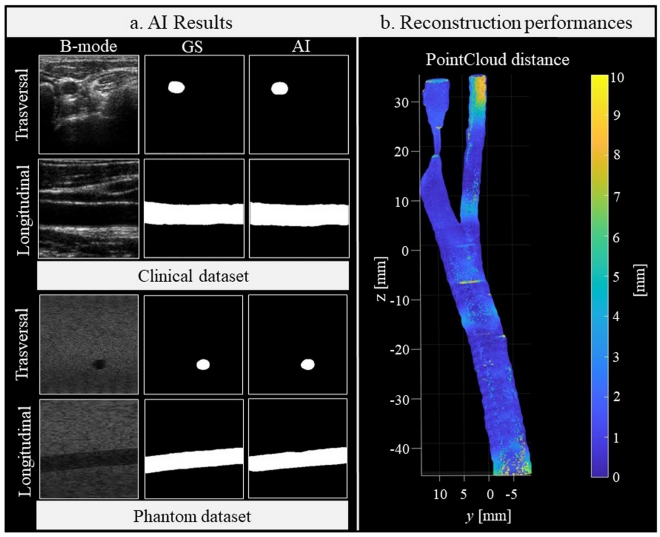

Fig. 4. Segmentation and reconstruction results. In panel a. the CNN results on the clinical and phantom datasets are shown, comparing original US B-mode images, GS annotations and CNN results. In panel b. the color distance map for 3D reconstruction of the CCA model is reported.

B. US-based Registration

Registration efficiency is crucial to exploit the pre-operative 3D model information and the trajectory automatically generated in the intra-operative stage, thus to properly conduct the intervention. Here we aim to validate our US-based approach by computing alignment errors when varying phantom orientation. The proposed method has been firstly validated in simulation, and then with experimental data. For simulation, cylindrical objects with different known radii and orientations have been generated to be compared with the reconstructed ones. This registration approach reported average radius and orientation estimation error of 0.92 pixel size and 0.74° (0.013 rad).

The experiments were then replicated considering 3 different relative orientations of the phantom with respect to the reference one (i.e., phantom rotated by 15°, 22.5° and 30°) and scanning the CCA portion which has a radius of about 4 mm. The performances with experimental data were 0.31 mm and 0.82° (0.014 rad). In Fig. 5 the experimental setup and the inertia-based output are depicted for the 30° phantom rotation.

C. Catheter Tracking and Automatic Insertion

Once registration has been carried out and the US probe has been longitudinally aligned to the target vessel, catheter insertion can take place. Automatic catheter drive is the result of two agent cooperation: catheter tracking and robotic arm control routine. The former should provide a feedback on catheter tip presence, while the latter should drive it as close as possible to the user defined target location. To evaluate the performance of the catheter tracking method, sensitivity and specificity metrics were computed. The former refers to the probability of null hypothesis correct rejection (i.e., the probability to correctly classify a ROI containing the catheter tip), the latter refers

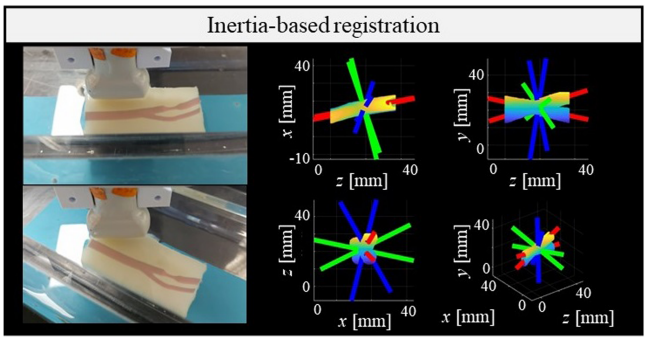

Fig. 5. Inertia-based registration experimental setup and results. On the right, two reconstructed point clouds with the estimated major axes are visible (blue and green for the transversal ones, red for the longitudinal one, used for orientation estimation).

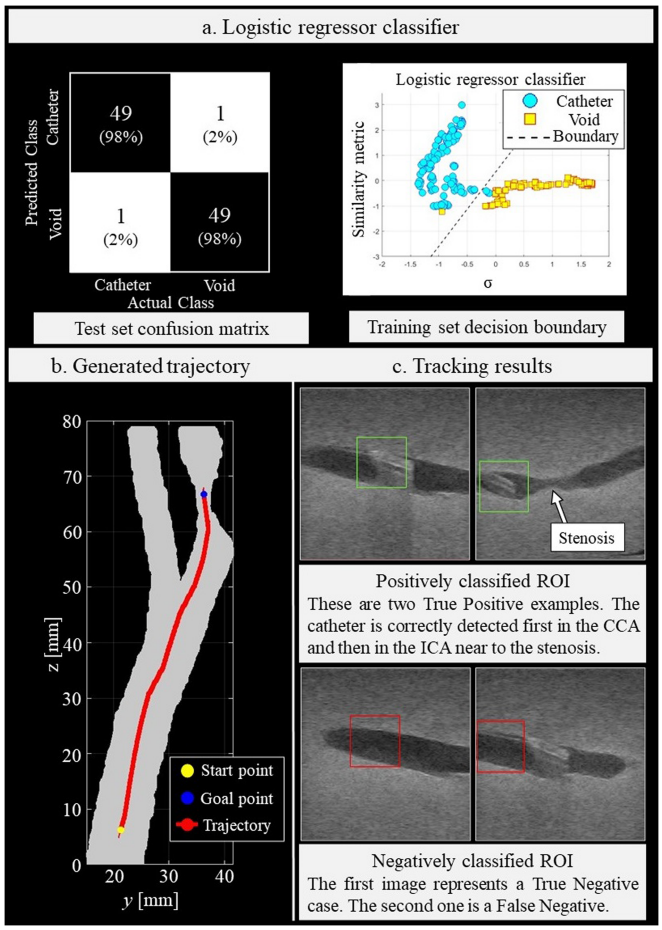

Fig. 6. Automatic catheter insertion. In panel a. details on logistic regressor classifier performances are reported. In panel b. an example of automatically generated trajectory is depicted and in panel c. some examples of the 2-player tracking strategy are visible.

to the probability of null hypothesis correct acceptance. The logistic regressor-based classifier reached sensitivity and specificity values both equal to 98%. Fig. 6(a) reports the confusion matrix on test set and the decision boundary on training set.

Control routine performance was evaluated thanks to a catheter drive experiment. A trajectory was automatically generated to drive the catheter tip from CCA bottom to ICA stenosis (Fig. 6(b)). Once the system was registered and aligned with the user-defined starting point, the centerline-based trajectory was followed to deliver the catheter to the target location. Trajectory point-to-point step l was set at 0.25 mm to guarantee optimal catheter dragging whereas the safety margin value n was set to 5. At each trajectory point, a frame was stored and analyzed by the 2-players tracker to allow closed-loop control (Fig. 6(c)). The distance of catheter tip to the center of ICA was computed as control error and turned out to be 3.3 mm.

IV. Discussion & Conclusion

In this letter, we presented a novel AI-enabled robotic platform for US-guided intravascular procedures, focusing on TCAR as a case study. Firstly, 3D vasculature is precisely reconstructed from 2D US images exploiting robotics and DL to enable pre-operative planning and intra-operative automatic guidance. The proposed approach is able to reach sub-millimeter reconstruction error (median error 0.95 mm), thus being comparable to US-based state-of-the-art methods for diagnosis [22], [23], but more precise than US-based vascular structure estimation methods currently exploited for control [9], [24], [25]. Secondly, a US-based registration routine has been developed to link pre- and intra-operative scenarios, a task which was lacking in latest works [8], [9], [24], [25]. This registration routine is based on the estimation of vessel pose from AI-based image segmentation and volume reconstruction. A similar pipeline was recently proposed in [38] for RGB-D camera-based industrial applications providing an orientation error of 0.035 rad. By exploiting inertia tensor for vessel pose estimation, we were able to reach lower orientation errors (0.014 rad) even if using lower quality images as US. This high precision registration is fundamental for optimal longitudinal vessel imaging and to correctly exploit 3D model information for out-of-plane movements. Last, Variable Structure Binary Feedback control for automatic navigation of a magnetic catheter has been demonstrated. To increase tracking precision and safety, we added a logistic regressor binary classifier in cascade to the template-matching tracker commonly exploited in catheter applications [8], [9], [25]. This enabled the discrimination of correct or faulty ROIs with sensitivity and specificity up to 98%. The magnetically guided catheter was able to go over vessel bifurcation reaching the ICA stenosis with a control error of 3.3 mm. Overall, the proposed RUS platform is able to reconstruct 3D vessel shapes from 2D US images with sub-millimetric performances in the pre-operative phase. Intra-operatively, vessel pose with respect to robot base frame is estimated from US images with sub-degree orientation errors and an automatic trajectory is followed to drive the small-scale catheter to the target location, optimally aligning the US probe with the vessel of interest. At this point, the operator can regain full control of the procedure to optimally go over the stenosis and subsequently place the stent under US guidance.

These promising results pave so the way for the robotization of TCAR procedure and an increased exploitation of US imaging with respect to CT, thus reducing patient and surgeon exposure to ionizing radiations, still achieving sub-millimetric anatomical volumes reconstruction, and standardizing the procedure. In the near future, we intend to improve system performances. Firstly,

force control for optimal probe-skin contact and patient safety should be included. This would allow to control probe elevation being compliant with patient neck curvature and guaranteeing optimal acoustic coupling. Secondly, the AI algorithm should be deployed on GPUs for real-time usage enabling, e.g., vessel lumen segmentation also during catheter insertion.

REFERENCES

[1] M. L. Flaherty et al., "Carotid artery stenosis as a cause of stroke," *Neuroepidemiology*, vol. 40, no. 1, pp. 36–41, 2013.

[2] A. D. Giannoukas, M. Chabok, K. Spanos, and A. Nicolaides, "Screening for asymptomatic carotid plaques with ultrasound," *Eur. J. Vasc. Endovascular Surg.*, vol. 52, no. 3, pp. 309–312, Sep. 2016.

[3] R. G. Nogueira et al., "Robotic assisted carotid artery stenting for the treatment of symptomatic carotid disease: Technical feasibility and preliminary results," *J. NeuroInterventional Surg.*, vol. 12, no. 4, pp. 341–344, 2020.

[4] J. H. Weinberg et al., "Comparison of robotic-assisted carotid stenting and manual carotid stenting through the transradial approach," *J. Neurosurgery*, vol. 135, no. 1, pp. 21–28, 2020.

[5] R. Abbas et al., "Robot-assisted carotid artery stenting: Outcomes, safety and operational learning curve," *Neurosurgical Focus*, vol. 52, no. 1, 2022, Art. no. E17.

[6] R. J. Webster, J. M. Romano, and N. J. Cowan, "Mechanics of precurved-tube continuum robots," *IEEE Trans. Robot.*, vol. 25, no. 1, pp. 67–78, Feb. 2009.

[7] K. H. Lee et al., "MR safe robotic manipulator for MRI-guided intracardiac catheterization," *IEEE/ASME Trans. Mechatron.*, vol. 23, no. 2, pp. 586–595, Apr. 2018.

[8] C. M. Heunis, Y. P. Wotte, J. Sikorski, G. P. Furtado, and S. Misra, "The ARMM system - autonomous steering of magnetically-actuated catheters: Towards endovascular applications," *IEEE Robot. Automat. Lett.*, vol. 5, no. 2, pp. 705–712, Apr. 2020.

[9] Z. Yang, L. Yang, M. Zhang, Q. Wang, C. H. Simon, and L. Zhang, "Magnetic control of a steerable guidewire under ultrasound guidance using mobile electromagnets," *IEEE Robot. Automat. Lett.*, vol. 6, no. 2, pp. 1280–1287, Apr. 2021.

[10] C. Fischer, Q. Boehler, and B. J. Nelson, "Using magnetic fields to navigate and simultaneously localize catheters in endoluminal environments," *IEEE Robot. Automat. Lett.*, vol. 7, no. 3, pp. 7217–7223, Jul. 2022.

[11] S. K. Zhou et al., "A review of deep learning in medical imaging: Imaging traits, technology trends, case studies with progress highlights, and future promises," *Proc. IEEE*, vol. 109, no. 5, pp. 820–838, May 2021.

[12] Y. Wang, X. Ge, H. Ma, S. Qi, G. Zhang, and Y. Yao, "Deep learning in medical ultrasound image analysis: A review," *IEEE Access*, vol. 9, pp. 54310–54324, 2021.

[13] A. A. Pravitasari et al., "UNet-VGG16 with transfer learning for MRI-based brain tumor segmentation," *TELKOMNIKA (Telecommun. Comput. Electron. Control)*, vol. 18, no. 3, Jun. 2020, Art. no. 1310.

[14] I. B. Ahmed, "Hybrid UNET model segmentation for an early breast cancer detection using ulrasound images," in *Proc. Conf. Comput. Collective Intell. Technol. Appl.*, 2022, pp. 464–476.

[15] F. von Haxthausen, S. Böttger, D. Wulff, J. Hagenah, V. García-Vázquez, and S. Ipsen, "Medical robotics for ultrasound imaging: Current systems and future trends," *Curr. Robot. Rep.*, vol. 2, no. 1, pp. 55–71, Mar. 2021.

[16] Q. Huang, J. Lan, and X. Li, "Robotic arm based automatic ultrasound scanning for three-dimensional imaging," *IEEE Trans. Ind. Inform.*, vol. 15, no. 2, pp. 1173–1182, Feb. 2019.

[17] S. Virga et al., "Automatic force-compliant robotic ultrasound screening of abdominal aortic aneurysms," in *Proc. IEEE/RSJ Int. Conf. Intell. Robots Syst.*, South Korea, 2016, pp. 508–513.

[18] F. Suligoj, C. M. Heunis, J. Sikorski, and S. Misra, "RobUSt–an autonomous robotic ultrasound system for medical imaging," *IEEE Access*, vol. 9, pp. 67456–67465, 2021.

[19] Z. Jiang, Y. Zhou, Y. Bi, M. Zhou, T. Wendler, and N. Navab, "Deformation-aware robotic 3D ultrasound," *IEEE Robot. Automat. Lett.*, vol. 6, no. 4, pp. 7675–7682, Oct. 2021.

[20] Z. Jiang et al., "Autonomous robotic screening of tubular structures based only on real-time ultrasound imaging feedback," *IEEE Trans. Ind. Electron.*, vol. 69, no. 7, pp. 7064–7075, Jul. 2022.

[21] M. A. Janvier, G. Soulez, L. Allard, and G. Cloutier, "Validation of 3D reconstructions of a mimicked femoral artery with an ultrasound imaging robotic system: 3D robotic ultrasound imaging," *Med. Phys.*, vol. 37, no. 7Part1, pp. 3868–3879, Jun. 2010.

[22] S. Merouche, L. Allard, E. Montagnon, G. Soulez, P. Bigras, and G. Cloutier, "A robotic ultrasound scanner for automatic vessel tracking and three-dimensional reconstruction of B-mode images," *IEEE Trans. Ultrasonics, Ferroelect., Freq. Control*, vol. 63, no. 1, pp. 35–46, Jan. 2016.

[23] L. A. Groves, B. VanBerlo, N. Veinberg, A. Alboog, T. M. Peters, and E. C. S. Chen, "Automatic segmentation of the carotid artery and internal jugular vein from 2D ultrasound images for 3D vascular reconstruction," *Int. J. Comput. Assist. Radiol. Surg.*, vol. 15, no. 11, pp. 1835–1846, Nov. 2020.

[24] C. Heunis, F. Šuligoj, C. F. Santos, and S. Misra, "Real-time multi-modal sensing and feedback for catheterization in porcine tissue," *Sensors*, vol. 21, no. 1, Jan. 2021, Art. no. 273.

[25] Z. Yang, L. Yang, M. Zhang, N. Xia, and L. Zhang, "Ultrasound-guided wired magnetic microrobot with active steering and ejectable tip," *IEEE Trans. Ind. Electron.*, vol. 70, no. 1, pp. 614–623, Jan. 2023.

[26] Neurosurgical Atlas, tag 36-37-39.Accessed: Oct. 30, 2022. [Online]. Available: https://www.neurosurgicalatlas.com/sketchfab?id=1a6a0fece597461b81a9f55e02317741

[27] J. Krejza et al., "Carotid artery diameter in men and women and the relation to body and neck size," *Stroke*, vol. 37, no. 4, pp. 1103–1105, Apr. 2006.

[28] A. Cafarelli, A. Verbeni, A. Poliziani, P. Dario, A. Menciassi, and L. Ricotti, "Tuning acoustic and mechanical properties of materials for ultrasound phantoms and smart substrates for cell cultures," *Acta Biomaterialia*, vol. 49, pp. 368–378, Feb. 2017.

[29] W. Wan, A. D. Bannerman, L. Yang, and H. Mak, "Poly(Vinyl Alcohol) cryogels for biomedical applications," in *Polymeric Cryogels*, vol. 263, O. Okay, Ed., Cham, Switzerland: Springer, 2014, pp. 283–321.

[30] J. Rouco, E. Azevedo, and A. Campilho, "Automatic lumen detection on longitudinal ultrasound B-mode images of the carotid using phase symmetry," *Sensors*, vol. 16, no. 3, pp. 350, Mar. 2016.

[31] P. Tamimi-Sarnikowski, A. Brink-Kjær, R. Moshavegh, and J. A. Jensen, "Automatic segmentation of vessels in in-vivo ultrasound scans," *Proc. SPIE*, Vol. 10137, pp. 446–454, Mar. 2017.

[32] S. Latha, D. Samiappan, P. Muthu, and R. Kumar, "Fully automated integrated segmentation of carotid artery ultrasound images using DBSCAN and affinity propagation," *J. Med. Biol. Eng.*, vol. 41, no. 2, pp. 260–271, Apr. 2021.

[33] M. Xie et al., "Vessel lumen segmentation in carotid artery ultrasounds with the U-net convolutional neural network," in *Proc. IEEE Int. Conf. Bioinf. Biomed.*, Seoul, Korea (South), Dec. 2020, pp. 2680–2684.

[34] M. Xie et al., "Two-stage and dual-decoder convolutional U-net ensembles for reliable vessel and plaque segmentation in carotid ultrasound images," in *Proc. 19th IEEE Int. Conf. Mach. Learn. Appl.*, Miami, FL, USA, Dec. 2020, pp. 1376–1381.

[35] N. Siddique, S. Paheding, C. P. Elkin, and V. Devabhaktuni, "U-Net and its variants for medical image segmentation: A review of theory and applications," *IEEE Access*, vol. 9, pp. 82031–82057, 2021.

[36] Ultrasound image database. Accessed Oct. 30, 2022. [Online]. Available: https://splab.cz/en/research/zpracovani-medicinskychsignalu/databaze/artery; 100-IMT-Images of the CCA, Accessed Oct. 30, 2022. [Online]. Available: https://www.researchgate.net/publication/261703132_100-IMT-Images_of_the_CCA

[37] J. Cao, A. Tagliasacchi, M. Olson, H. Zhang, and Z. Su, "Point cloud skeletons via Laplacian based contraction," in *Proc. Shape Model. Int. Conf.*, France, Jun. 2010, pp. 187–197.

[38] H. Xu, G. Chen, Z. Wang, L. Sun, and F. Su, "RGB-D-based pose estimation of workpieces with semantic segmentation and point cloud registration," *Sensors*, vol. 19, no. 8, Apr. 2019, Art. no. 1873.